applied sciences

MDPI

Article

Uncertainty Quantification for Thermodynamic Simulations with High-Dimensional Input Spaces Using Sparse Polynomial Chaos Expansion: Retrofit of a Large Thermal Power Plant

Roeland De Meulenaere [1,2,*], Diederik Coppitters [3], Ale Sikkema [4], Tim Maertens [4] and Julien Blondeau [1,2]

[1] Thermo and Fluid Dynamics (FLOW), Faculty of Engineering, Vrije Universiteit Brussel (VUB), Pleinlaan 2, 1050 Brussels, Belgium; julien.blondeau@vub.be
[2] Brussels Institute for Thermal-Fluid Systems and Clean Energy (BRITE), Vrije Universiteit Brussel (VUB) and Université Libre de Bruxelles (ULB), 1050 Brussels, Belgium
[3] Institute of Mechanics, Materials and Civil Engineering (iMMC), Université Catholique de Louvain (UCLouvain), Place du Levant, 2, 1348 Louvain-la-Neuve, Belgium; diederik.coppitters@uclouvain.be
[4] Onyx Power, Missouriweg 69, 3199 LB Maasvlakte, The Netherlands; ale.sikkema@onyx-power.com (A.S.); tim.maertens@onyx-power.com (T.M.)
* Correspondence: roeland.de.meulenaere@vub.be

Abstract: The assessment of the future thermodynamics performance of a retrofitted heat and power production unit is prone to many uncertainties due to the large number of parameters involved in the modeling of all its components. To carry out uncertainty quantification analysis, alternatives to the traditional Monte Carlo method must be used due to the large stochastic dimension of the problem. In this paper, sparse polynomial chaos expansion (SPCE) is applied to the retrofit of a large coal-fired power plant into a biomass-fired combined heat and power unit to quantify the main drivers and the overall uncertainty on the plant's performance. The thermodynamic model encompasses over 180 components and 1500 parameters. A methodology combining the use of SPCE and expert judgment is proposed to narrow down the sources of uncertainty and deliver reliable probability distributions for the main key performance indicators (KPIs). The impact of the uncertainties on each input parameter vary with the considered KPI and its assessment through the computation of Sobol' indices. For both coal and biomass operations, the most impactful input parameters are the composition of the fuel and its heating value. The uncertainty on the performance and steam quality parameters is not much affected by the retrofit. Key furnace parameters exhibit a skewed probability distribution with large uncertainties, which is a strong attention point in terms of boiler operation and maintenance.

Keywords: uncertainty quantification; biomass; retrofit; CHP

Citation: De Meulenaere, R.; Coppitters, D.; Sikkema, A.; Maertens, T.; Blondeau, J. Uncertainty Quantification for Thermodynamic Simulations with High-Dimensional Input Spaces Using Sparse Polynomial Chaos Expansion: Retrofit of a Large Thermal Power Plant. *Appl. Sci.* **2023**, *13*, 10751. https://doi.org/10.3390/app131910751

Academic Editor: Tomohiro Tabata

Received: 31 August 2023
Revised: 22 September 2023
Accepted: 22 September 2023
Published: 27 September 2023

1. Introduction

Worldwide, many scientists are conducting research on new electricity production methods, such as solar [1], wind [1], hydro [1], tidal [1], algae [2], bio-fuel [3], geothermal [4], etc., as well as on energy storage [5,6], such as carbon capture and storage (CCS) [7] and carbon capture and utilization (CCU) [8] to decrease the impact of electricity production on the climate [9,10] and the resulting global temperature increasing [11]. Currently, a substantial part of our electricity is still produced with coal-fired power plants [12]. Could these existing assets be converted to biomass to decrease their CO_2 emissions and contribute to mitigating climate change? Such a conversion would indeed result in a short-term, significant reduction of their CO_2 footprint [13]. Later, when more intermittent renewable energy is available, grid stability can be perpetuated using biomass fired power plants as back up for wind and solar energy. Although it sometimes remains a controversial topic, which falls out of the scope of this work, studies have confirmed the potential contribution of such retrofits to global CO_2 emission reduction policies [14–16].

While co-firing of biomass with fossil fuels is intensely researched nowadays [17–19], it is more difficult to find studies about full coal-to-biomass conversions [20–22]. Assessing the future thermodynamics performance of retrofitted heat and power production plants is, however, not straightforward. It requires a detailed modeling of complex processes and their components. In this paper, the impact on the performance of a retrofit of a coal-fired power plant into a biomass combined heat and power (CHP) and the working method is discussed.

In [23], we modeled and optimised the retrofit of a large-scale ultra-supercritical (USC) coal-fired power plant into a biomass-fired CHP unit using a deterministic thermodynamic model made of 180 components, 285 links, and 1500 variables. Key performance indicators (KPIs) were defined and assessed. A shortcoming of the deterministic comparison between 100% coal and 100% biomass CHP for different loads and different temperatures of the heat-to-heat clients is that uncertainties were not taken into account.

A widely employed technique for uncertainty quantification (UQ) is the fundamental Monte Carlo simulation method. This approach involves the random generation of scenarios based on input parameter distributions until a sufficient quantity, typically ranging from 10^4 to 10^5, of output values is accumulated. This dataset serves as a robust statistical distribution of potential outcomes [24]. However, this method encounters challenges when the system model requires more than a few seconds to produce results for each scenario [25].

To enhance computational efficiency, surrogate-assisted UQ leverages a surrogate model of the system. This surrogate model simplifies the system's representation within the bounds defined by the various input parameter distributions. Examples of surrogate models encompass Kriging [26], support vector machines [27], analysis of variance (ANOVA) [28], and polynomial chaos expansion (PCE) [29]. PCE, for example, enables the analytical derivation of distribution parameters and sensitivity indices, such as Sobol' indices, from the surrogate model's coefficients. Ref. [30] describes a probabilistic comparison between an USC coal-fired power plant before and after a conversion to biomass. In this paper, the possibility of uncertainty quantification (UQ) polynomial chaos expansion (PCE) is investigated to avoid the issue of unknown parameters. PCE was applied on two unknown parameters related to heat transfer in the furnace of the boiler.

In traditional PCE, the truncation set contains multivariate polynomials, many of which represent interactions between input variables. However, in engineering scenarios, high-interaction term coefficients (those representing interactions between multiple uncertain parameters) are often negligible, as physical phenomena are primarily driven by main effects and low-order interactions [31]. Consequently, determining these high-interaction coefficients through deterministic model evaluations is inefficient. In the truncation scheme, a substantial number of coefficients correspond to high-interaction terms in the PCE. For instance, in a case with a stochastic dimension of 50 and a maximum polynomial degree of 3, the number of terms in $\mathcal{A}^{50,3}$ is 23,426. Within this set, only 150 polynomials depend on a single random parameter (univariate polynomials), which is less than 1% of the total. Accordingly, many coefficients can be considered negligible and should not significantly impact the computational cost of constructing the PCE, aligning with the sparsity-of-effect principle [32]. In line with this principle, sparse PCE methods have been developed to identify significant coefficients a priori [33].

Initially, sparse PCE algorithms emerged within the context of compressive sensing [34]. Compressive sensing methods enabled the retrieval of a sparse solution with fewer design samples than basis functions [33]. Regression-based sparse PCE was first introduced using a forward–backward selection procedure [32]. An alternative truncation scheme was proposed by [35], where only multivariate polynomials dependent on a limited number of input parameters are included. The number of input parameters on which multivariate polynomials may depend is a user-defined constant established a priori. A more relevant approach is least-angle regression (LAR) [35], which utilizes a hyperbolic truncation scheme to exclude terms with high-interaction order. Recently, Abraham et al. [36] introduced a stepwise regression method that adaptively determines

significant terms from the basis functions pool, promising improved sparsity and accuracy in sparse PCE compared to LAR.

In this paper, the performance of the USC coal-fired power plant at 100% load (current situation) is compared with the low temperature biomass CHP at 80% load (best case in [23]) using the stepwise sparse PCE algorithm proposed by Abraham et al. [36]. The goal of this paper is to address this question: "How can the performance of complex thermodynamic systems be evaluated under uncertainty?". The following are the next steps:

1. The definition of a methodology to apply advanced uncertainty quantification techniques to process modeling involving large numbers of parameters and several KPIs.
2. Apply this methodology to the case of a retrofitted, large biomass CHP unit.
3. Investigation of the limits of uncertainty quantification (UQ) polynomial chaos expansion (PCE) and, finally, sparse PCE.
4. Investigation of the most important parameters to model both cases.

Currently, the coal-fired power plant runs at base load as much as possible; therefore, the studied load for the coal-based operation is 100%. The research in [23] revealed that running the biomass CHP system at 80% load, with a CHP efficiency of 67%, is the most effective mode of operation. This will also be the preferred operating mode after conversion, and in this study the load of the biomass-based operation will be 80%.

2. Materials and Methods

2.1. Thermodynamic Modeling and Validation

The power plant considered in this study is an USC coal-fired power plant located in the Netherlands and commissioned in 2015. The 730 MW_e power plant has a net electrical efficiency of 45%. The power plant is fed with coal that will be crushed in one of the four roller mills. When the particles of the coal are little enough they will be taken by the primary air to one of the four low-NO_x burners in the burner row of that mill. Thus, there are four burner rows of four burners in an opposed-type arrangement in this 1550 MW_{th} boiler. The combustion air is pressurized by two forced-draught (FD) fans and passes through a rotary air preheater to recuperate energy from the flue gasses. After combustion, the flue gasses are forced through a state-of-the-art flue gas treatment (FGT) system by an induced draught (ID) fan. The FGT exists for a selective catalytic reduction (SCR) denitrification system, an electrostatic precipitator (ESP) to remove the dust, and a wet scrubber to reduce the SO_x emissions. The USC boiler contains an economizer, three super heaters, and two reheaters, and the walls are the evaporator ("evaporator " is the customary term for the radiative heat exchanger in the furnace, although the cycle is supercritical in this case and, therefore, does not present an evaporation phase as such). The feedwater that arrives in the economizer comes from the condenser, and between the condenser and the economizer, the feedwater flows through five low-pressure preheaters, a deaerator, and three high-pressure preheaters. The feedwater is pressurized by several pumps after the condenser and after the deaerator. The steam, 252.2 bar and 600 °C, coming from the outlet of the super heaters, flows through a high-pressure steam turbine. In the reheaters, the steam still has a pressure of 61 bar and is upgraded to 620 °C before the steam is led to the intermediate pressure steam turbine. After the intermediate pressure steam turbine, the steam flows to one of the two double-flow low-pressure steam turbines. Afterwards, the used steam is condensed in one of the two water-cooled condensers. In total, there are nine extractions out of the steam turbines to heat the feedwater in the preheaters. The water steam cycle is visualized in a simplified overview in Figure 1.

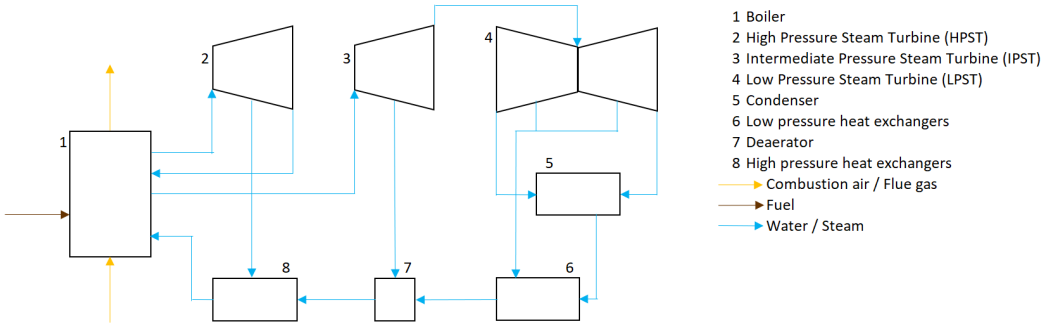

Figure 1. Simplified schematic of the steam cycle [23].

The power plant is modeled with Thermoflex®. Thermoflex® is a high-fidelity fully flexible engineering software application for modeling and simulating the thermodynamic behavior of power production facilities (CCGT, CFPP, nuclear, renewables, etc.) and is the most flexible and adaptable package of Thermoflow®. The software is state-of-the-art heat and mass balance software featuring a graphical user interface. In the design mode, the model can be made by using the over two hundred different predefined components. After component selection and connection, the default values of the components can be adapted and Thermoflex® computes the full heat and mass balance and the performances of the entire system, based on a series of thermodynamic design assumptions. Switching to the next mode, Thermoflex® translates the initial basic thermodynamic design assumptions into physical realistic components. Afterwards the model can be frozen in off-design mode and static simulations can be performed. The software calculates first all the pressures in the system, and when an equilibrium is reached, all the flows will be calculated followed by all the other parameters. With the ELINK application, the model can be made quasi-dynamic [23,30,37]. The basic model illustrated in Figure 1 corresponds to the current, coal-based operation, while the extended model illustrated in Figure 2 also comprises the additional steam extractions from the three tapping points (outlet HP, outlet IP, and LP turbines) to an intermediate closed loop via heat exchangers (elements 9 to 11) required for combined heat and power (CHP) production. This intermediate loop in turns delivers heat to the heat clients (element 12). The model will be used to simulate the following operational modes:

1. The current situation: the fuel is coal; the power plant runs base load.
2. Potential new situation: the fuel is biomass; the power plant runs at a boiler load of 80%, and there is low-temperature heat extraction in the CHP extension.

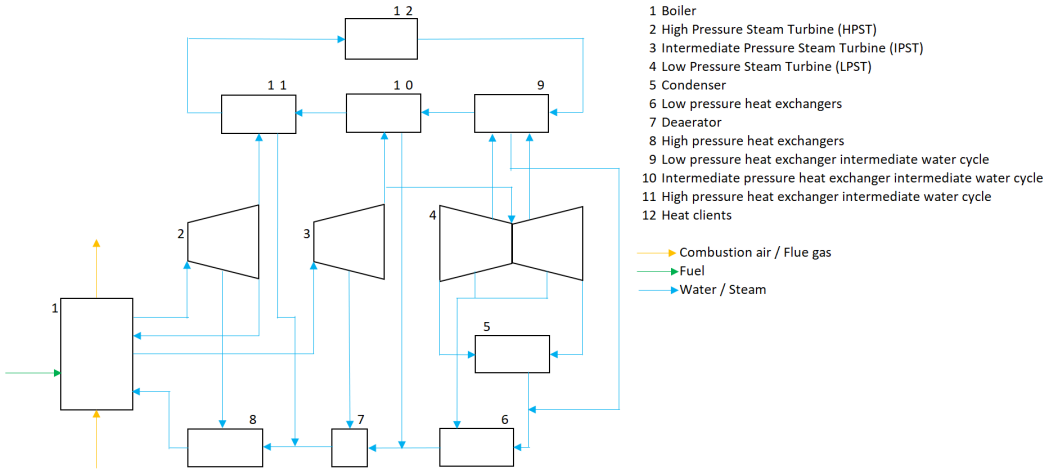

Figure 2. Overview CHP.

The biomass used is steam-exploded pellets, because the structure is comparable with coal, and only a new classifier and an ATEX fuel system will be needed, while for traditional white pellets, heavier modifications of the storage, handling, and milling systems are required. This results in a lower investment cost to retrofit the power plant. Compared with white pellets, the other advantages of steam-exploded pellets are the higher lower heating value (LHV) and the fact that they are hydrophobic [38–40]. On the other hand, there is the higher price of the steam-exploded pellets. Whether these higher operational costs can be counterbalanced by the reduced investment costs is a function of the operation of the power plant: a low capacity factor will indeed favor the option of lower investments and higher operational costs. A part of the higher operational costs can be regained by the additional production of heat and valuable chemical compounds during pellet production [41]. Although the higher LHV of steam-exploded pellets (20,060 kJ/kg) is still significantly lower than the LHV of coal (24,221 kJ/kg).

In the previous works [23,30], we developed thermodynamic models of the coal-fired power plant using Thermoflex®. First, the coal-fired power plant was modeled at base load and validated against the official acceptance test. This model was then used to build several other models for the lower loads, which were validated against performance test conducted by the experts of the power plant around the time of the acceptance test. Using the available operational data gathered over 5 years of operation, the aging was implemented in the base case model and validated against performance tests executed by the power plant experts. Later on, the same aging was implemented in the lower load models. Afterwards, the fuel of the models was changed from coal to biomass and the results were validated against biomass co-firing test runs. In [30], the thermodynamic models are used to study the impact of furnace heat transfer parameter uncertainties with UQ PCE, and it is shown that experimental results are within the calculated uncertainty bounds. These models are used as the basis for this study.

The steam turbine was originally designed to allow steam extraction for district heating (DH) purposes. Three extraction points are available: from the HP turbine outlet (cold reheat line), from the IP turbine outlet, and from the LP turbine. The latter extraction point is specifically designed for large flow rates, unlike the four other conventional steam extraction points from the LP turbine delivering heat to the feedwater preheaters in order to increase the efficiency of the steam cycle. The design of the turbine is such that it can deliver 150 MW_{th} of thermal power to a DH network at maximum continuous rate (MCR) load, assuming a supply temperature to the network of 180 °C and a return temperature of 80 °C [23]. Nevertheless, the limitation of maximum steam extraction of 150 MW_{th} is not taken into account for this study. The conditions of the extracted steam and returned condensate can be found in Table 1 and results in a supply and return temperature for the external heat client of 70 °C and 30 °C, respectively [23].

Table 1. Conditions of the extracted steam and the returned condensate.

Extraction	Pressure [bar]	Temperature [°C]	Flow [kg/s]	Enthalpy [kJ/kg]
LP extraction	3.07	278	44	3025
Return	1.67	49.75	44	208.4
IP extraction	5.275	339.2	31	3145
Return	13.8 [1]	110.5	31	464.4
HP extraction	50.68	393.9	104	3180
Return	49.69	151.1	104	639.8

[1] The return pressure is higher than the extraction pressure because there is a pump in the process return system.

2.2. Uncertainty Characterization

2.2.1. Selection of Uncertain Input Parameters

In the process of configuring the power plant simulations using Thermoflex®, a comprehensive set of inputs is necessitated. While some of these inputs are mandatory, others remain optional as they are initialized with default values by the software. In collaboration with the power plant experts, a detailed analysis of all 1500 of input parameters inherent to the model was conducted. This analysis started by removing certain hardware parameters (e.g., materials of tubes in the heat exchangers, length and amount of tubes in the boiler, setpoints, design values such as deaerator and condenser pressure, etc.) from the list of all 1500 input parameters. Next, the independence of the uncertain input parameters was checked. The parameters that are dependent on each other were removed after they were grouped into one overall uncertainty parameter. Finally, the input parameters affecting only the low load have been removed. This analysis led to the identification of all parameters that are subject to uncertainty due to inherent variability or lack of information, and associated with appropriate probability distributions, including uniform, logarithmic, and n-logarithmic distributions. The prescribed distributions were delineated by their respective ranges, occasionally augmented by lower and upper bounds depending on the inherent characteristics of the distribution. For the current situation with coal, the final list contains 242 parameters and for the biomass case, 243 parameters were detected. A more detailed description of the most impactful parameters is provided in Section 3.1, and the comprehensive list with all the parameters is available in the Supplementary Materials.

2.2.2. Selection of Outputs

Numerous potential output parameters were available for selection; however, the interdependence between different outputs, as well as their reliance on shared input parameters, necessitated a discerning approach. Consequently, outputs were chosen that provide insight on power plant performance as parameters and parameters of intrinsic importance to the power plant and its operation but that are not, difficult or only indirectly measurable. So the selected output parameters are divided in three groups: plant performance indicators, steam quality indicators, and furnace operation indicators. The selection of the output parameters can be found in Table 2. The first trio of parameters, namely gross power, gross efficiency, and CHP efficiency, is an obvious choice. These output parameters provide a good picture of the impact of the retrofit on the power plant performance and are indispensable for estimating both the financial implications as well as the generation of electricity and heat after the conversion. The next two parameters are the pressure and flow of the steam leaving the boiler and entering the high-pressure steam turbine. These two output parameters provide better insights into the quality of high-pressure steam and the potential capacity loss of the boiler and steam turbine due to changes in fuel type and different LHV due to fuel source modifications. The last three output parameters are adiabatic flame temperature, furnace exit gas temperature (FEGT) and effective radiation temperature. These parameters are important because they are difficult or impossible to measure [42]; nevertheless, these parameters significantly affect combustion dynamics and kinetics within the boiler, especially in the case of a fuel retrofit. These parameters influence factors such as soot formation and the distribution of heat exchange mechanisms, more precisely, the interaction between radiation and convection. The soot formation will initiate slagging and fouling issues which are very undesirable because coal and biomass fired power plants are very sensitive to it [43,44].

Table 2. Selected outputs.

# Output	Output Variable Description	Unit
Plant performance indicators		
1	Plant gross power	MW
2	Plant gross electric efficiency	%
3	Plant CHP efficiency	%
Steam quality indicators		
4	Live steam pressure	bar
5	Live steam flow rate	kg/s
Furnace operation indicators		
6	Adiabatic flame temperature	°C
7	Furnace exit gas temperature (FEGT)	°C
8	Effective radiation temperature	°C

2.3. Uncertainty Quantification

Once the distributions for the input parameters are set (Section 2.2.1), uncertainty quantification (UQ) comes into play. It involves carrying over these input distributions through the system model and gauging the uncertainty in a specific output (Section 2.2.2).

In light of the considerable time cost associated with model evaluation (approximately 90 s) and the substantial number of uncertainties (243), we have opted for an approach that employs sparse polynomial chaos expansion. This method helps us propagate uncertainty, calculate statistical moments, and find global sensitivity indices (Sobol' indices) for indicators of the plant's performance [36]. The Python-based RHEIA framework is used to connect the developed Thermoflex® models to the relevant robust optimization algorithms described below [45].

2.3.1. Construction of the PCE

Like in a conventional PCE [25], the surrogate model (M^{PCE}) replicates the relation between the input parameters and the output parameter of interest defined in the Thermoflex® model (M). This PCE representation consists of a truncated series of multivariate orthonormal polynomials $\mathbf{\Psi}$ weighted by coefficients u:

$$M^{\mathrm{PCE}}(\boldsymbol{\xi}) = \sum_{i=0}^{P} u_i \mathbf{\Psi}_i(\boldsymbol{\xi}) \approx M(\boldsymbol{\xi}), \tag{1}$$

where $\boldsymbol{\xi} = (\xi_1, \xi_2, \ldots \xi_n)$ represents the vector of the independent random parameters, and d corresponds to the number of input distributions. Typically, the number of multivariate polynomials in the series is limited by the maximum total degree of the multivariate polynomials (p) and the number of uncertain parameters (d). The number of multivariate polynomials that correspond to an order below or equal to the limiting order p equals:

$$P + 1 = \binom{p+d}{p} = \frac{(d+p)!}{d!p!}. \tag{2}$$

The number of terms ($P + 1$) in the truncated series using the conventional truncation scheme increases dramatically when $d > 10$ (i.e., *curse-of-dimensionality*) [25]. To illustrate, for $d = 243$ and a limiting degree p of 2 and 3, the number of multivariate polynomials in the series equals 29,890 and 2,450,980, respectively.

Each multivariate polynomial in the series is accompanied by a coefficient. To quantify the values of these coefficients, a regression method is adopted [25]. To acquire a well-posed least-square minimization, the empirical rule of thumb is to have a number of training samples equal to at least two times the number of coefficients [25]. As these training samples are evaluated in the true simulation model (M), the construction of a PCE using

the conventional truncation scheme becomes computationally intractable (i.e., roughly 7 years for $p = 3$ without parallelization).

2.3.2. Sparse Polynomial Chaos Expansion

Not all uncertain input parameters carry equal weight in influencing the variance of the output. This inherent sparsity in the relationship between inputs and outputs can result in a substantial reduction in the number of terms needed in the expansion. Moreover, many models exhibit a pattern where they can be effectively represented by main effects and low-order interactions, adhering to the sparsity of effects principle. Consequently, a significant portion of coefficients in the polynomial chaos expansion (PCE) may approximate to zero [36].

To address this challenge and mitigate the computational cost associated with constructing a conventional PCE, an approach is to detect non-negligible terms in the PCE before its actual construction. To this end, we employed the sparse polynomial chaos expansion (sparse PCE) algorithm, as described in Abraham et al.'s work [36]. This approach efficiently identifies and retains the most influential terms, substantially reducing the computational burden while maintaining the accuracy necessary for robust uncertainty quantification. Hence, this algorithm focuses on retaining only the most impactful coefficients and their associated polynomials in the truncated series. For a comprehensive visual representation of this method, readers can refer to the schematic diagram available in Abraham et al.'s work [36].

The initial step of the algorithm involves creating an initial design of experiment, denoted as $\chi = [\boldsymbol{\xi}^1, \boldsymbol{\xi}^2, ..., \boldsymbol{\xi}^n]$, where the user-defined constant n determines its size. The experiment's design is evaluated using the true model, and the resulting output for the quantity of interest is stored in $\boldsymbol{y} = [y_1, y_2, ..., y_n]^T$. In the first forward step, the algorithm creates and evaluates $P + 1$ independent one-predictor regression models using individual basis functions. The assessment is performed by solving a least-squares problem.

To select the preferred basis function $\boldsymbol{\Psi}_{j*}$ out of the $P + 1$ one-predictor regression models, the following criterion is applied:

$$j* = \text{argmax}_j \frac{|\hat{u}_j|}{\sqrt{\text{Var}[\hat{u}_j]}}, \quad j = 0, ..., P, \tag{3}$$

where $\hat{u}_j$ represents the estimate of the coefficient and $\text{Var}[\hat{u}_j]$ corresponds to its variance. This criterion favors coefficients with high weights (i.e., high estimates) in most of the samples (i.e., low variances), as they carry the most significant information. This selection procedure ensures effectiveness and robustness. The best-performing one-predictor model is stored in the final regression model, and it is removed from the pool of basis functions. The residual $\hat{\boldsymbol{e}}$ is updated based on the difference between the deterministic model results $\boldsymbol{y}$ and the results from the final regression model at the design of experiment points $\hat{\boldsymbol{y}}$:

$$\hat{\boldsymbol{e}} = \boldsymbol{y} - \hat{\boldsymbol{y}}. \tag{4}$$

Following the first forward step, the stepwise regression algorithm enters a forward–backward loop. The forward step is similar to the first forward step, except that the one-predictor regression models are fitted on the residual $\hat{\boldsymbol{e}}_i$ at iteration i. This fitting on the residual enables the models to capture the effects that are still missing in the final regression model. After each forward step, a backward step is initiated. In this backward step, the confidence intervals of the regression coefficients included in the regression model are evaluated to determine if the importance of the coefficients already in the model is affected by the entry of a new coefficient. The confidence interval is computed as follows:

$$u_i \in \left[\hat{u}_i \pm z[1 - \alpha/2]\sqrt{\text{Var}(\hat{u}_i)}\right], \tag{5}$$

where $\mathrm{Var}(\hat{u}_i)$ represents the i-th diagonal term of $\mathrm{Var}(\hat{\boldsymbol{u}})$, $z[1-\alpha/2]$ is the $1-\alpha/2$ quantile of the standard normal distribution, and α is set to 0.05. If a confidence interval includes 0, the corresponding coefficient is removed from the model, and the residual is updated. This process is repeated until the maximum number of iterations is reached. For further details on this sparse PCE method, refer to Abraham et al. [36].

2.3.3. Error Estimation

To estimate the error of the PCE, we employ leave-one-out (LOO) cross-validation. In LOO, one sample $\boldsymbol{x}^{(i)}$ is excluded from the set of n random samples, and the PCE is constructed without this sample's information, denoted as $\mathcal{M}^{\mathrm{PCE}\setminus i}$. The residual error at that point is defined as the difference between the result from the actual model $\mathcal{M}$ and the result from the PCE without the information on that point $\mathcal{M}^{\mathrm{PCE}\setminus i}$:

$$\Delta_i \;=\; \mathcal{M}\left(\boldsymbol{x}^{(i)}\right) - \mathcal{M}^{\mathrm{PCE}\setminus i}\left(\boldsymbol{x}^{(i)}\right). \tag{6}$$

The residual error can be quantified by leaving out each sample, one at a time, from the set of samples to construct the PCE. Since n samples are present in the set, the LOO error corresponds to the sum of the n residual errors:

$$E_{\mathrm{LOO}} \;=\; \frac{1}{n}\sum_{i=1} n\Delta_i^2. \tag{7}$$

Hence, this technique consistently leaves one sample out during each iteration and constructs a PCE surrogate model with one fewer samples. This meticulous process ensures that our PCE surrogate model is rigorously validated against test data that were not utilized during the training phase. However, this approach involves constructing n PCEs, which can be computationally demanding in large stochastic dimensions. However, based on algebraic derivations [25], the LOO error can be quantified using the i-th diagonal terms in the matrix $\boldsymbol{A}\left(\boldsymbol{A}^{\mathrm{T}}\boldsymbol{A}\right)^{-1}\boldsymbol{A}^{\mathrm{T}}$. Eventually, the LOO error is given by

$$E_{\mathrm{LOO}} \;=\; \frac{1}{n}\sum_{i=1}^{n}\left(\frac{\mathcal{M}(\boldsymbol{x}(i)) - \mathcal{M}^{\mathrm{PCE}}(\boldsymbol{x}(i))}{1-h_i}\right). \tag{8}$$

It should be noted that in this formulation, $\mathcal{M}^{\mathrm{PCE}}$ is constructed based on the full experimental design (i.e., n samples). The LOO error can be normalized by dividing it by the variance of the model outputs $\mathrm{Var}[\boldsymbol{y}]$.

2.3.4. Post-Processing

The statistical moments can be derived from the PCE coefficients analytically, i.e., no more model evaluations are required. To illustrate, the mean μ^{PCE} and standard deviation σ^{PCE} are derived as follows (higher moments could also be obtained):

$$\mu^{\mathrm{PCE}} = u_0, \tag{9}$$

$$\sigma^{2\ \mathrm{PCE}} = \sum_{\boldsymbol{\alpha}\in\mathcal{A},\boldsymbol{\alpha}\neq\mathbf{0}} u_{\boldsymbol{\alpha}}^2. \tag{10}$$

Next to the statistical moments, the Sobol' indices (i.e., global sensitivity indices) can be derived from the PCE coefficients as well. The Sobol' indices represent the decomposition into fractions of the variance of the quantity of interest, for which each fraction is allocated to a random input parameter (first order) or a set of random input parameters (higher order). The total-order Sobol' indices (S_i^T) are quantified as follows:

$$S_i^T \;=\; \sum_{\boldsymbol{\alpha}\in A_i^T} u_{\boldsymbol{\alpha}}^2 \Big/ \sum_{i=1}^{P} u_i^2 \qquad A_i^T \;=\; \{\boldsymbol{\alpha}\in A | \alpha_i > 0\}, \tag{11}$$

where A is the set of all the PCE coefficients and α_i represents the coefficient related to uncertain parameter i.

2.3.5. Characterization

The sparse PCE methodology is governed by two user-defined parameters: the total degree of multivariate polynomials and the number of training samples. The determination of both these parameters follows the approach proposed by Abraham et al. [36]. Initially, the process begins with setting the total degree parameter to $p = 1$ and then gradually increasing the number of training points. For each set of training points, a sparse PCE is systematically constructed, and subsequently, the LOO error is assessed. This iterative procedure continues until the LOO error reaches a point of convergence or until all multivariate polynomials from the pool of basis functions limited by $p = 1$ (as per Equation (2)) are incorporated into the PCE. Should the LOO error exceed a predefined threshold, the total degree parameter is incremented to $p = 2$, thereby introducing additional polynomials into the basis function pool. This iterative process continues until the combination of polynomial order and the number of training samples yields an LOO error that falls below the established threshold.

In this work, we selected a limiting polynomial degree $p = 3$, in combination with a design of experiment of 5000 training points (χ) to reach an LOO error below 1% for all outputs of interest (see Section 2.2.2). This accuracy corresponds to the accuracy of the PCE model achieved in previous work of these authors [30], where a LOO error below 1% is achieved for $p = 3$ on the same power plant simulation model. However, the number of training samples required is significantly higher (5000, as opposed to 20 in [30]), and, as in this work, the number of uncertain parameters is several orders of magnitude higher (243, as opposed to 2). In addition, the gain in computational efficiency by applying sparse PCE instead of the conventional PCE is similar to the one obtained in a recent application to a renewable energy system [46]. To illustrate the evolution of the LOO error with respect to the number of training samples, the evolution of the LOO error and the statistical moments of the coal-fired power plant gross power quantified by the sparse PCE (μ^{PCE} and $\sigma^{2\ \text{PCE}}$) with respect to the size of the design of experiment are presented in Figure 3 and Figure 4, respectively. The figures with all the LOO errors can be found in the Supplementary Materials.

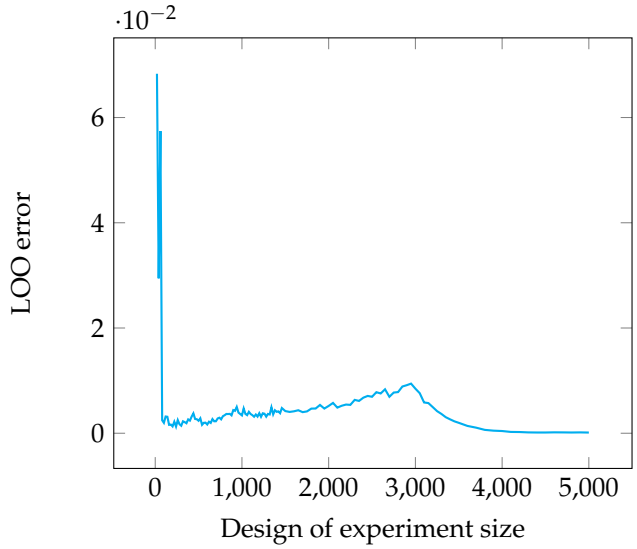

Figure 3. The evolution of the LOO error of the PCE for the coal-fired plant gross power with respect to the size of the design of experiment.

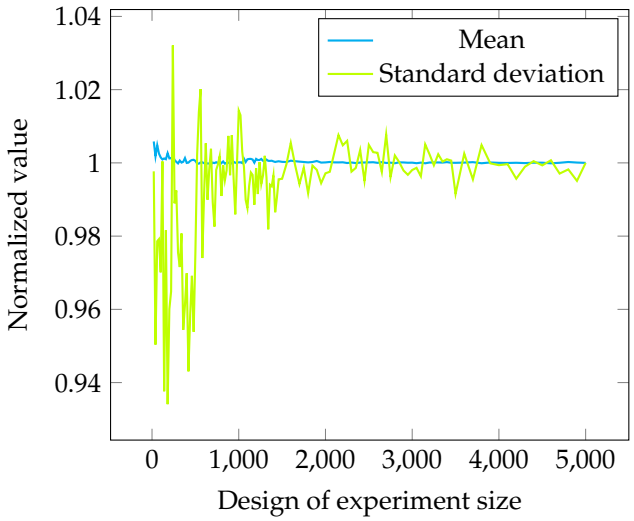

Figure 4. The evolution of the quantified mean and standard deviation of the coal-fired plant gross power with respect to the size of the design of experiment.

3. Results and Discussion

3.1. General Summary of the Results

Using a quasi-random Sobol' sampling, 5000 training samples are generated on the 242 uncertain parameters for coal-based operation and 243 uncertain parameters for biomass-based operation, while the other parameters are consider fixed. These samples are simulated with the Thermoflex® models. In the course of the study, a relevant observation emerged: not all output parameters depend (equally) on the same input parameters. This insight highlights the need to conduct specific analyses for each individual output, given the varying sensitivities to underlying input parameters. Therefore, SPCE surrogate models for each output parameter have been constructed using the deterministic response of the Thermoflex® simulations. The summary of the comparison between coal 100% load and biomass CHP 80% load of the resulting means and standard deviations can be found in Table 3.

Table 3. Summary of the resulting means and standard deviations of the simulations of the power plant before and after the conversion.

Output		Coal	Biomass	Unit
Plant gross power	mean	703	382	MW
	std	17.2	15.9	MW
Plant gross electric efficiency	mean	45.4	30.8	%
	std	1.1	1.3	%
Plant CHP efficiency	mean	41.5	65.3	%
	std	1.4	1.5	%
Live steam pressure	mean	235	185	bar
	std	14.2	7.9	bar
Live steam flow rate	mean	543	411	kg/s
	std	53.1	21.7	kg/s
Adiabatic flame temperature	mean	2026	1839	°C
	std	327	279	°C
FEGT	mean	1276	1132	°C
	std	73.6	52.8	°C
Effective radiation temperature	mean	1655	1489	°C
	std	201	166	°C

There are 18 input parameters with Sobol' index (impact) above 1% for at least one of the output parameters for both scenarios, and 17 of the 18 impactful input parameters are the same for both fuels (see Table 4). The order of importance of the input parameters per output parameter are shown in Table 5 for coal and in Table 6 for biomass and will be discussed in Section 3.2.

Table 4. Input parameters with Sobol' index above 1% for at least one output.

Fuel
Solid-fuel-weight percent of moisture
Solid-fuel-weight percent of ash
Solid-fuel-weight percent of C
Solid-fuel-weight percent of H
Solid-fuel-weight percent of S (only for coal)
Solid-fuel-specified LHV @ 25C
Furnace
Evaporator steam outlet temperature
Flue gas O_2 content
Waterwall radiant flux correction factor
Carbon-to-soot conversion rate
Ash emissivity exponent correction factor
Ash particle mean diameter
Non-uniform radiant flux factor
Radiant cooler: minor heat loss
Gas/air side convective heat transfer coefficient adjustment factor—SH1
Gas/air side convective heat transfer coefficient adjustment factor—SH2
Gas/air side convective heat transfer coefficient adjustment factor—SH3
Combustion air
Rotary air heater: cleanliness factor
Water/steam
High-pressure preheater 3: condensing zone heat transfer coefficient correction factor (only for biomass)

The fuel parameter 'weight percent of S' has a significant impact only in the case of coal, and the parameter 'high-pressure preheater 3: condensing zone heat transfer coefficient correction factor' has a significant impact only in the case of biomass.

3.2. Analysis Outputs

In this paragraph, for all the outputs, the effects of converting the power plant from coal to biomass CHP are discussed.

3.2.1. Plant Performance Indicators

Plant Gross Power

The gross power is of course the main parameter to study. As expected and in line with the choice to optimize the global CHP efficiency after the retrofit (see Section 2.1 and [30]), the mean decreases from 703 MW to 382 MW (see Figure 5). The standard deviation is rather low and has a negligible decrease from 17.17 MW for coal to 15.95 MW for biomass (see Figure 5); thus, the expected power is not more uncertain after the retrofit. Nevertheless, the relative standard deviation (mean versus standard deviation) of biomass is higher than the relative standard deviation of coal, which is in line with what was observed in [30].

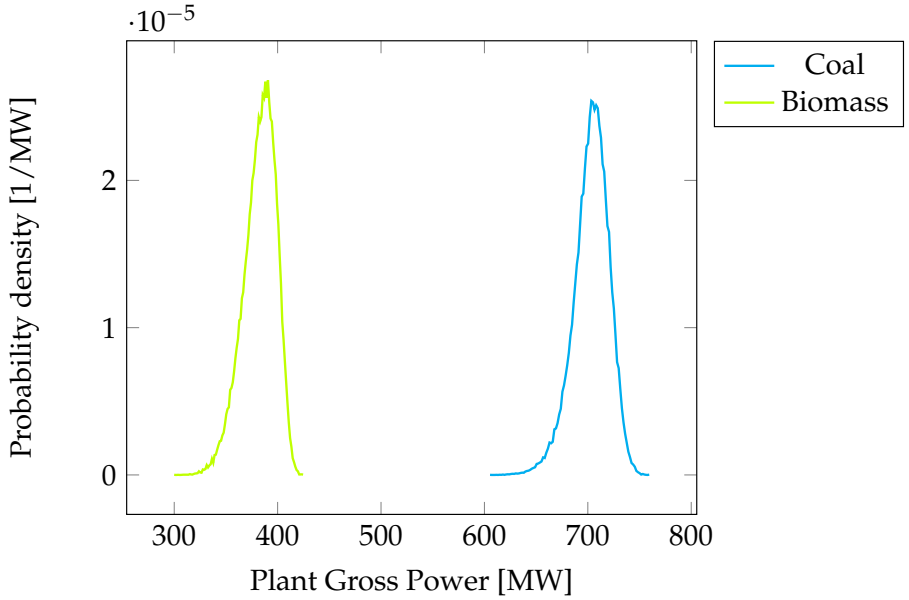

Figure 5. Gross power. Coal: mean = 703.2 MW, standard deviation = 17.1 MW. Biomass: mean = 382.3 MW, standard deviation = 15.8 MW.

Plant Gross Electric Efficiency

Another important parameter is the gross efficiency. As expected, the efficiency decreases from 45.3% to 30.8% (see Figure 6), just as for the gross power; these results are in line with the chosen CHP operation mode (see Section 2.1 and [30]). The uncertainty slightly increases from 1.1% to 1.3%, showing again that the overall performance of the plant will not be more uncertain after the retrofit (see Figure 6).

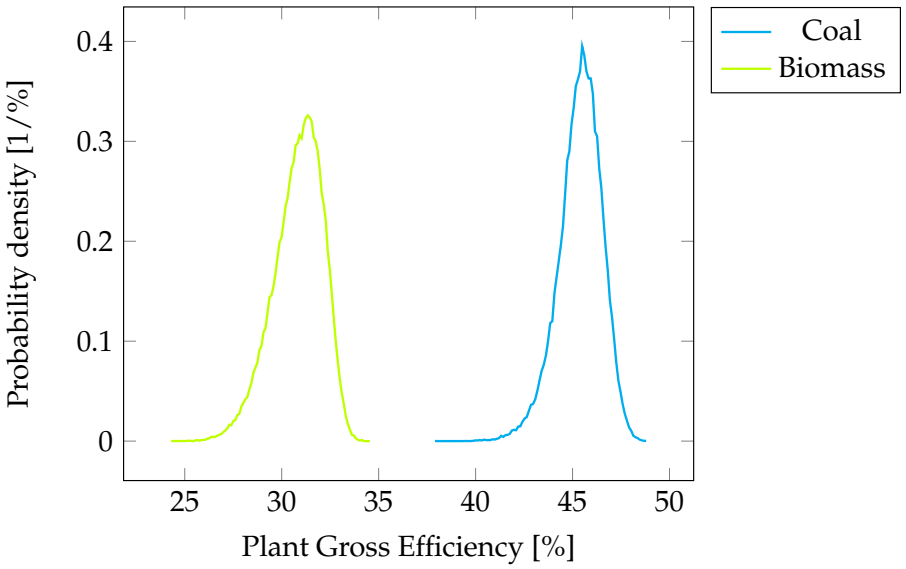

Figure 6. Gross efficiency. Coal: mean = 45.3%, standard deviation = 1.1%. Biomass: mean = 30.8%, standard deviation = 1.3%.

Plant CHP Efficiency

The CHP efficiency increases from 41.5% to 65.3% and the standard deviation from 1.4% to 1.5% (see Figure 7). The plant CHP efficiency (η_{CHP}) is calculated by summing the produced net electrical power ($P_{el,net}$) and the delivered thermal power as two equivalent forms of energy:

$$\eta_{CHP} = \frac{P_{el,net} + P_{th}}{P_{fuel}} \text{ [-]} \quad (12)$$

where P_{th} is the thermal power delivered to the heat client and P_{fuel} is the thermal power input in the boiler, calculated as the product of the fuel flow rate and its LHV. Because the coal-fired power plant only delivers electricity to the grid, while the biomass CHP also delivers heat to the DH, the CHP efficiency will obviously increase after conversion. Again, the expected performances are not much more uncertain after the retrofit.

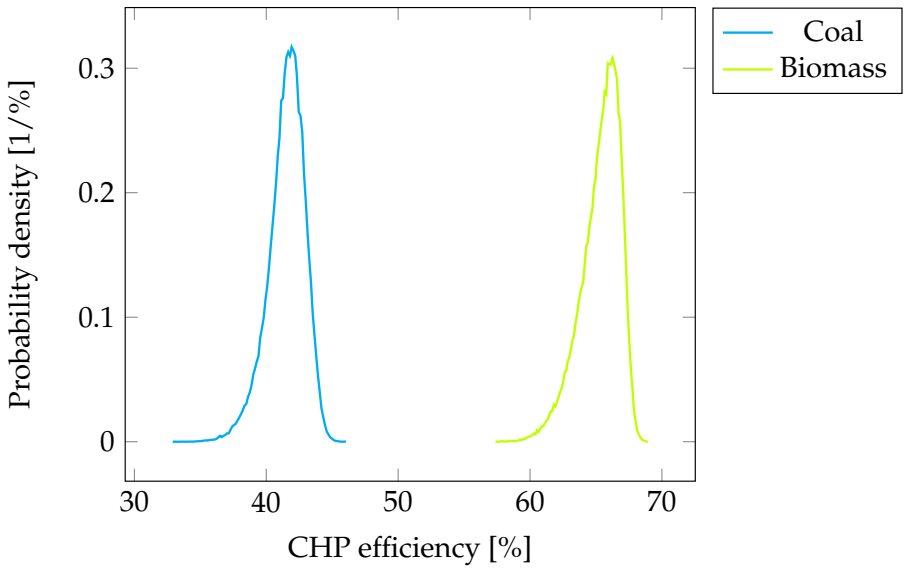

Figure 7. CHP efficiency. Coal: mean = 41.5%, standard deviation = 1.4%. Biomass: mean = 65.3%, standard deviation = 1.5%.

3.2.2. Steam Quality Indicators

Live Steam Pressure

The steam pressure to the high-pressure steam turbine decreases from 235 to 182 bar (see Figure 8). Due its lower LHV and higher moisture content, the combustion of biomass generates relatively more flue gas than the combustion of coal. This results in a lower adiabatic flame temperature and therefore in a less radiant heat transfer. As a consequence, reaching the nominal steam temperature cannot be achieved without decreasing the nominal steam pressure and steam flow rate. Considering the provided fuel thermal input, the control system of the power plant is programmed to first reach the nominal steam temperature considering the steam pressure and flow rates as secondary parameters.

While the power plant conversion from coal to biomass results in a steam pressure decrease, the related uncertainty decreases from 14 to 8 bar (see Figure 8) due to a higher sensitivity of this output on the composition of the fuel in the case of coal (especially on carbon content); see Section 3.3.1, Table 5 and Section 3.3.2, Table 6. The higher sensitivity to the LHV of biomass compared to coal does not compensate this effect.

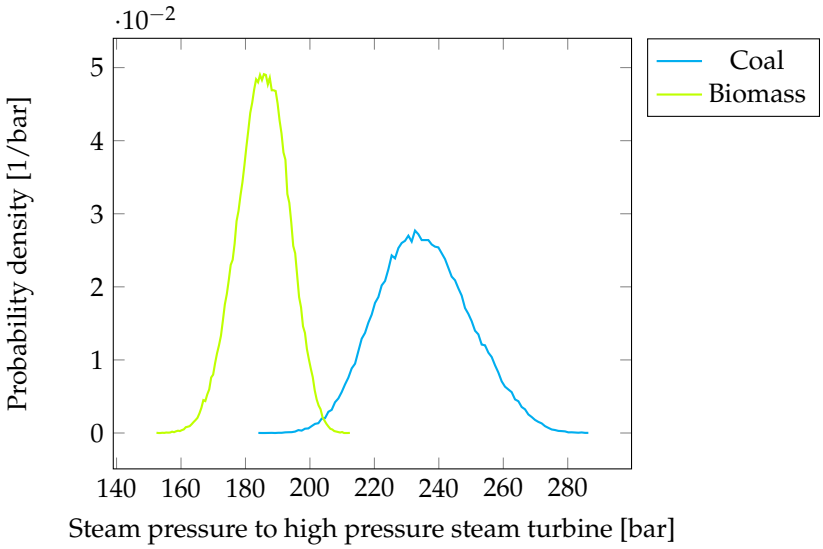

Figure 8. Steam pressure to high-pressure steam turbine. Coal: mean = 235 bar, standard deviation = 14 bar. Biomass: mean = 185 bar, standard deviation = 8 bar.

Live Steam Flow Rate

The same effects as for live steam pressure can be observed for live steam flow rate. The steam flow to the high-pressure steam turbine decreases from 542 to 410 kg/s and the uncertainty from 53 to 22 kg/s (see Figure 9), also due to a higher sensitivity of this output on the composition of the fuel in the case of coal, combined with a higher impact of evaporator steam outlet temperature; see Section 3.3.1, Table 5 and Section 3.3.2, Table 6.

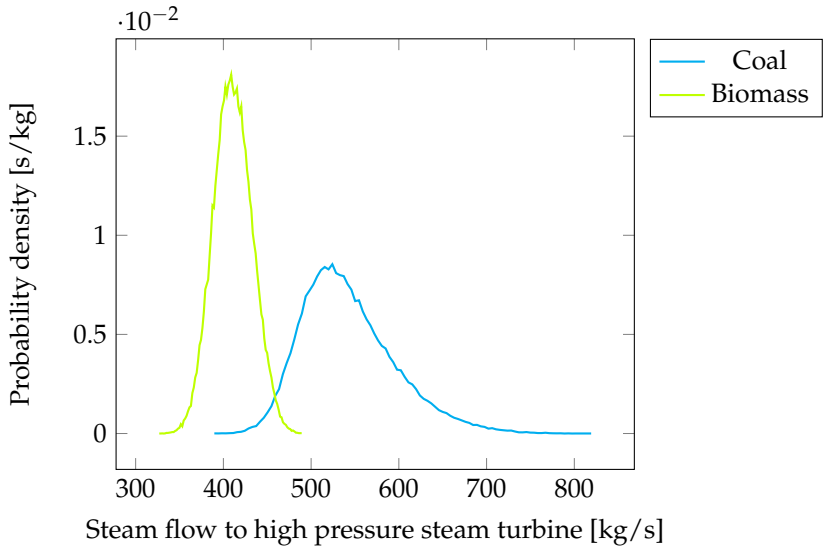

Figure 9. Steam flow to high-pressure steam turbine. Coal: mean = 542 kg/s, standard deviation = 53 kg/s. Biomass: mean = 410 kg/s, standard deviation = 22 kg/s.

3.2.3. Furnace Operation Indicators

Adiabatic Flame Temperature

The adiabatic flame temperature decreases from 2026 to 1839 °C, while the standard deviation decreases from 326 to 279 °C (see Figure 10). The higher moisture content, the lower LHV, and the higher amount of flue gas from biomass combustion lead to this temperature decrease. Compared to the previous parameters, the adiabatic flame temperature exhibits a much larger uncertainty for both coal and biomass but slightly lower for biomass. This parameter is mainly impacted by the uncertainty on the fuel composition;

see Section 3.3.1, Table 5 and Section 3.3.2, Table 6. The skewness of the distribution is also more pronounced, with a tail reaching significantly higher values than the mean. This can have important consequences for the operation and the maintenance of the boiler.

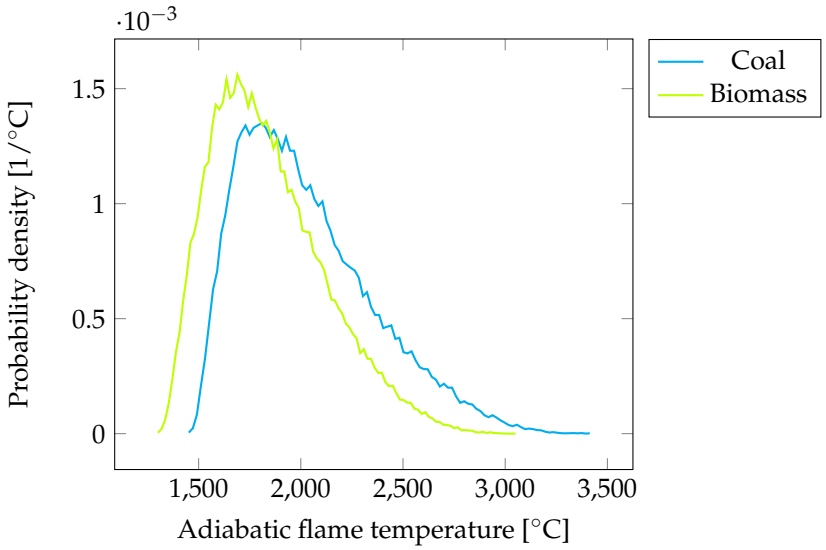

Figure 10. Adiabatic flame temperature. Coal: mean = 2026 °C, standard deviation = 326 °C. Biomass: mean = 1839 °C, standard deviation = 279 °C.

Furnace Exit Gas Temperature (FEGT)

The FEGT decreases from 1276 to 1131 °C (see Figure 11). Because the relatively higher flue gas flow for biomass, the radiative heat transfer in the furnace will decrease, but the convective heat transfer will increase. Nevertheless, the increased convection will not counterbalance the decreased radiation. A lower FEGT will positively impact the risk of slagging and fouling, which, however, mainly depends on the composition of the ash. This expected decrease can, however, be taken into account in ash deposition risk assessments. Also, the standard deviation is narrower for biomass (52.6 °C) than for coal (73.6 °C) (see Figure 11). Both are also mainly affected by the uncertainty on the composition of the fuel.

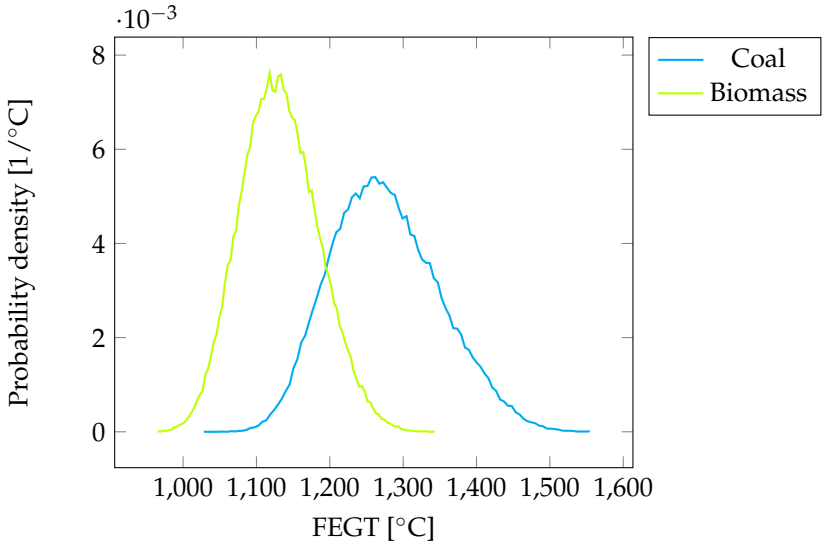

Figure 11. FEGT. Coal: mean = 1276 °C, standard deviation = 73.6 °C. Biomass: mean = 1131 °C, standard deviation = 52.6 °C.

Effective Radiation Temperature

The effective radiation temperature decreases from 1655 to 1489 °C, while the uncertainty decreases from 200 to 166 °C (see Figure 12). The effective radiation temperature is a heat-weighted average between the adiabatic flame temperature (see Paragraph 'Adiabatic Flame Temperature' in Section 3.2.3) and the FEGT (see Paragraph 'Furnace Exit Gas Temperature (FEGT)' in Section 3.2.3) [37]. This evolution can therefore be explained by the evolution of the two previous output parameters. The probability distribution of the adiabatic flame temperature, however, dominates and leads to a skewed distribution with a significant standard deviation for this parameter as well. As this parameter gives an image of the radiative heat transfer in the furnace, such a large uncertainty is concerning in terms of operation and maintenance of the boiler. The risk of tube failure because of excessive heat transfer is real in such large boilers. These results tend to show that the accurate monitoring of the combustion process in the furnace is key to ensuring a smooth operation of the power plant.

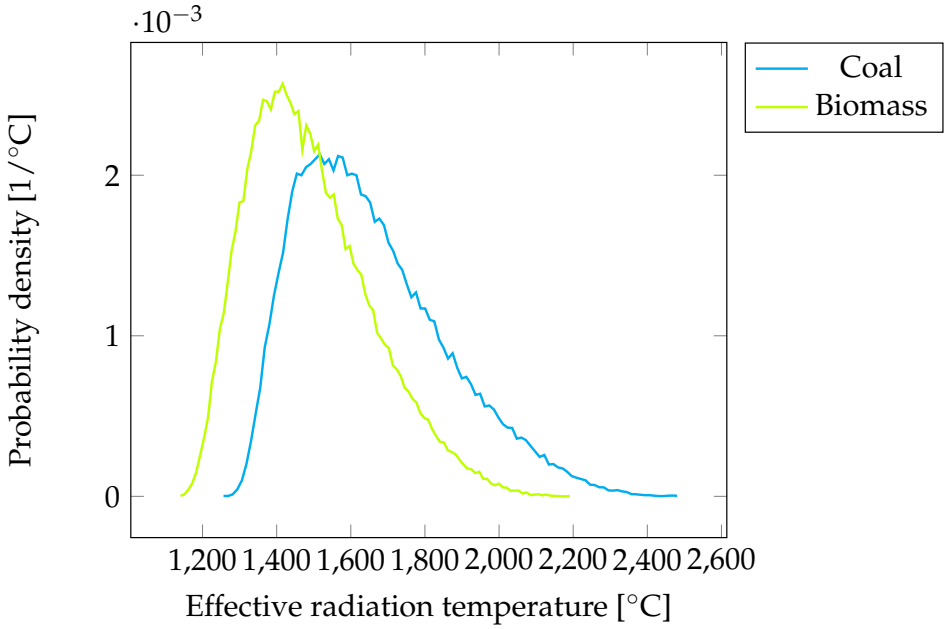

Figure 12. Effective radiation temperature. Coal: mean = 1655 °C, standard deviation = 200 °C. Biomass: mean = 1489 °C, standard deviation = 166 °C.

3.3. Analysis Inputs

In this section, the inputs (Table 4) will be discussed. Per input parameter ranked above 1% in the Sobol' analysis, a potential reason is discussed. All graphs can be found in the Supplementary Materials.

3.3.1. Coal:

Carbon and hydrogen content in the fuel are the two most impactful input parameters (see Table 5). Together, they have a minimum impact of 64.67% for the 'gross power' output and a maximum impact of 90.35% for the 'adiabatic flame temperature'. The next two important input parameters are 'evaporator steam outlet temperature' and 'LHV' for the outputs 'gross power' (respectively, 12.86% and 8.69%), 'gross efficiency' (respectively, 12.86% and 8.75%), 'steam flow' (respectively, 15.94% and 6.57%) and 'CHP efficiency' (respectively, 10.64% and 11.24%). The impact of the other input parameters for this outputs is lower than 3%. The 'LHV' input is also impactful for all the other parameters ('steam pressure': 7.90%, 'adiabatic flame temperature': 8.75%, 'effective radiation temperature': 8.86%, 'FEGT': 8.66%). The 'steam pressure' also depends on 'superheater 3: gas/air side

convective heat transfer coefficient adjustment factor' (3.96%), while the ash percentage is more impactful for 'FEGT' (5.59%). All the other inputs have an impact lower than 3%.

In general, the plant performance indicators mainly depend on the carbon and hydrogen content of the fuel and its LHV; also, the evaporator outlet temperature has an impact on these outputs. The steam quality indicators are influenced by the carbon and hydrogen content of the fuel and the live steam flow rate output also by the evaporator outlet temperature. The furnace operation indicators are also mainly influenced by the carbon and hydrogen content of the fuel and its LHV. Of course, it is expected that the carbon and hydrogen content and the LHV of the fuel would have a big impact, but it is surprising that the influence is that big compared with all the other input parameters. The evaporator steam outlet temperature is the only other parameter that has a reasonable impact on the output. This temperature ultimately determines the final energy content of the steam to the steam turbines; the lower this temperature is, the lower the final steam temperature will be, which explains why this input parameter impacts only the plant performance indicators and the live steam pressure.

3.3.2. Biomass:

For all the biomass outputs, the three most important input parameters are carbon and hydrogen content and the LHV of the fuel (see Table 6). For the first three outputs, 'gross power', 'gross efficiency' and 'CHP efficiency', the 'LHV' has more impact than the 'hydrogen' input. The three parameters together have an impact of 75.99% for the 'FEGT' output, while the impact for the 'adiabatic flame temperature' is 98.81%. For all the others, the sum of the impact is in between these two parameters. For the 'FEGT' output, the input 'carbon-to-soot conversion rate' parameter has an impact of 6.42%. The impact of 'weight percentage ash' (4.76%), 'waterwall radiant flux correction factor' (4.77%) and 'non-uniform radiant flux factor' (4.32%) can also have some impact but are already significantly lower. For all the other inputs, the impact on the outputs is lower than 4%.

Comparison of the results of the Sobol' indices for coal and biomass shows that the carbon and hydrogen content of the fuel and the LHV of the fuel are the most impactful input parameters for both. Only for some output parameters of coal, the evaporator steam outlet temperature has also a certain impact, while this input parameter has no influence on the same output parameters in the biomass case. As explained in Paragraph 'Plant Gross Power' in Section 3.2.1, the nominal steam temperature cannot be achieved without decreasing the nominal steam pressure and steam flow rate in the biomass case. It seems that the evaporator steam outlet temperature only has influence on the output parameters when the nominal steam parameters are reached.

Table 5. Sobol' indices in % of the impactful input parameters per output parameter for coal.

	Plant Gross Power	Plant Gross Electric Efficiency	Plant CHP Efficiency	Live Steam Pressure	Live Steam Flow Rate	Adiabatic Flame Temperature	FEGT	Effective Radiation Temperature
Fuel								
Solid-fuel-weight percent of moisture						1.65		1.53
Solid-fuel-weight percent of ash	1.04	1.17	2.39			1.48	5.59	2.02
Solid-fuel-weight percent of C	37.60	38.48	39.37	44.43	40.21	53.63	44.86	53.03
Solid-fuel-weight percent of H	27.07	27.06	27.40	29.21	27.36	36.71	29.23	35.90
Solid-fuel-weight percent of S			2.60					
Solid-fuel-specified LHV @ 25C	8.69	8.75	11.24	7.90	6.57	8.75	8.66	8.86
Furnace								
Evaporator steam outlet temperature	12.86	12.87	10.64	1.48	15.94			
Flue gas O_2 content		1.02	1.11	1.08		1.09		1.05
Waterwall radiant flux correction factor							2.05	
Carbon-to-soot conversion rate							2.79	
Ash emissivity exponent correction factor							1.17	
Ash particle mean diameter							2.11	
Non-uniform radiant flux factor							2.07	
Radiant cooler: minor heat loss	2.83	2.90	1.57					
Gas/air side convective heat transfer coefficient adjustment factor—SH1				1.40				
Gas/air side convective heat transfer coefficient adjustment factor—SH2	2.64	1.97	1.02	3.96	1.19			
Gas/air side convective heat transfer coefficient adjustment factor—SH3				2.98	2.42			
Combustion air								
Rotary air heater: cleanliness factor	2.55	2.51	1.87					

Table 6. Sobol' indices in % of the impactful input parameters per output parameter for biomass.

	Plant Gross Power	Plant Gross Electric Efficiency	Plant CHP Efficiency	Live Steam Pressure	Live Steam Flow Rate	Adiabatic Flame Temperature	FEGT	Effective Radiation Temperature
Fuel								
Solid-fuel-weight percent of moisture	1.04	1.08	1.26	1.00	1.14	1.41		1.40
Solid-fuel-weight percent of ash			1.93			1.41	4.77	1.75
Solid-fuel-weight percent of C	22.65	22.71	24.33	23.62	23.17	31.76	24.03	31.44
Solid-fuel-weight percent of H	38.44	38.29	37.09	36.80	37.09	45.98	32.85	44.94
Solid-fuel-specified LHV @ 25C	24.20	24.10	27.91	19.38	19.02	21.08	19.10	21.29
Furnace								
Evaporator steam outlet temperature					2.19			
Flue gas O_2 content	1.21	1.25	1.43	1.15	1.14	1.16		1.13
Waterwall radiant flux correction factor							4.23	
Carbon-to-soot conversion rate							6.43	
Ash emissivity exponent correction factor							1.38	
Ash particle mean diameter							2.02	
Non-uniform radiant flux factor							4.32	
Radiant cooler: minor heat loss	2.50	2.35	1.50					
Gas/air side convective heat transfer coefficient adjustment factor—SH1				3.05	2.48			
Gas/air side convective heat transfer coefficient adjustment factor—SH2				3.90	2.41			
Gas/air side convective heat transfer coefficient adjustment factor—SH3				1.82	1.79			
Combustion air								
Rotary air heater: cleanliness factor	3.19	3.16	2.16	1.15				
Water/steam								
High-pressure preheater 3: condensing zone heat transfer coefficient correction factor					1.02			

3.4. Limitations of the Study

The sparse PCE method is founded on the assumption of independence among the random input parameters. This assumption, while simplifying the mathematical framework and computational implementation of the PCE, is a limitation when dealing with systems or processes where input parameters are not strictly independent. However, the independence assumption can still provide valuable insights and reasonably accurate results for systems where correlations among input parameters are not highly significant. Moreover, PCE can be employed as a tool for sensitivity analysis, helping to identify which input parameters have the most influence on the system's output, even under the independence assumption. In situations where strong correlations among input parameters exist, more advanced techniques, such as Copula-based modeling or surrogate modeling methods, that can handle correlated inputs may be considered. These approaches can provide a more accurate representation of the system's behavior when independence among inputs cannot be assumed. Therefore, while the independence assumption of PCE is a limitation, its applicability and usefulness persist in various scenarios, making it a valuable tool in uncertainty quantification and sensitivity analysis.

4. Conclusions

The conversion from a base-load coal-fired power plant into an 80%-load biomass CHP will, as expected, result in a gross power decrease from 703 to 382 MW and a gross electric efficiency decrease from 45.4% to 30.8%, while the CHP efficiency increases from 41.5% to 65.3%. The uncertainty of these parameters stays more or less the same before and after the conversion. The steam quality indicators and furnace operation indicators also decrease after conversion, and all the related standard deviations decrease too, which shows that these parameters tend to be less uncertain for biomass than for coal combustion. Among the furnace parameters, the adiabatic flame temperature and the effective radiation temperature, however, show significant uncertainties and skewed probability distributions. This is a strong attention point in terms of boiler operation and maintenance. With the analysis of the Sobol' indices, it is shown that only 18 of the 242 input parameters for coal and 243 input parameters for biomass have a significant impact on the studied outputs, and 17 of the 18 impactful input parameters are the same for coal and biomass, but only 4 input parameters strongly dominate the impact on the uncertainties for coal outputs: carbon and hydrogen content of the fuel, LHV of the fuel, and the evaporator outlet temperature. For biomass, only 3 high impact input parameters are observed: carbon and hydrogen content of the fuel and LHV of the fuel. In this work, it is shown that the proposed methodology, combining expert judgment and SPCE for numerous unknown inputs and multiple outputs, can be used to assess the performances of complex thermodynamics systems under uncertainty. This method can be used to avoid a lack of information for high-fidelity simulation programs such as Thermoflex®. If the retrofits of several similar power plants have to be modeled and simulated, the computational time can be drastically reduced after the first power plant is calculated because attention can be focused on the important input parameters, namely the input parameters with the highest Sobol' indices for the next power plants. In future works, the methodology should be applied to investigate the impact of daily and seasonal load changes on the performance of the power plant. Given the importance of the fuel characteristics, conversions to other bio-fuels, e-fuels, or their mixtures could also be investigated, including in other types of thermal assets that will play a role in future energy systems, such as combined cycles. Financial and carbon footprint aspects could be included as well in the KPIs. The use of stochastic processes could be investigated [47,48].

Supplementary Materials: The following supporting information can be downloaded at: https://www.mdpi.com/article/10.3390/app131910751/s1, The list of variable input parameters and the corresponding distributions for coal and biomass, all resulting data for coal and biomass, all resulting data of the LOOs and all the resulting Sobol indices, with supplementary graphs of the results.

Author Contributions: Conceptualization, R.D.M., D.C., A.S. and J.B.; Methodology, R.D.M., D.C., A.S. and J.B.; Software, R.D.M. and D.C.; Validation, R.D.M., D.C. and A.S.; Formal analysis, R.D.M., D.C. and A.S.; Investigation, R.D.M. and D.C.; Resources, R.D.M., A.S. and T.M.; Data curation, R.D.M., D.C. and A.S.; Writing–original draft, R.D.M. and D.C.; Writing–review & editing, D.C., A.S. and J.B.; Visualization, R.D.M. and D.C.; Supervision, T.M. and J.B.; Project administration, R.D.M.; Funding acquisition, J.B. All authors have read and agreed to the published version of the manuscript.

Funding: This research was partly funded by the European Union's Horizon 2020 research and innovation program grant number 818349 and the Fonds de la Recherche Scientifique—FNRS [CR 40016260].

Institutional Review Board Statement: Not applicable.

Informed Consent Statement: Not applicable.

Data Availability Statement: We have published all our data and results in the Supplementary Material.

Acknowledgments: Part of the results presented in this paper were generated within the EU-H2020 project "Cost-effective transformation of a highly-efficient advanced thermal ultra-supercritical coal-fired power plant into a CHP by retrofitting and integrating an ARBAFLAME biomass upgrading process", with the acronym ARBAHEAT. This project has received funding from the European Union's Horizon 2020 research and innovation program under grant agreement No. 818349. Diederik Coppitters acknowledges the support of the Fonds de la Recherche Scientifique—FNRS [CR 40016260].

Conflicts of Interest: The authors declare no conflict of interest.

References

1. Ang, T.Z.; Salem, M.; Kamarol, M.; Das, H.S.; Nazari, M.A.; Prabaharan, N. A comprehensive study of renewable energy sources: Classifications, challenges and suggestions. *Energy Strategy Rev.* **2022**, *43*, 100939. [CrossRef]
2. Ahmad, S.; Iqbal, K.; Kothari, R.; Singh, H.M.; Sari, A.; Tyagi, V. A critical overview of upstream cultivation and downstream processing of algae-based biofuels: Opportunity, technological barriers and future perspective. *J. Biotechnol.* **2022**, *351*, 74–98. [CrossRef] [PubMed]
3. Hassan, M.H.; Kalam, M.A. An Overview of Biofuel as a Renewable Energy Source: Development and Challenges. *Procedia Eng.* **2013**, *56*, 39–53. [CrossRef]
4. Ciriaco, A.E.; Zarrouk, S.J.; Zakeri, G. Geothermal resource and reserve assessment methodology: Overview, analysis and future directions. *Renew. Sustain. Energy Rev.* **2020**, *119*, 109515. [CrossRef]
5. Ould Amrouche, S.; Rekioua, D.; Rekioua, T.; Bacha, S. Overview of energy storage in renewable energy systems. *Int. J. Hydrog. Energy* **2016**, *41*, 20914–20927. . [CrossRef]
6. Olabi, A.; Abdelkareem, M. Energy storage systems towards 2050. *Energy* **2021**, *219*, 119634. [CrossRef]
7. Tan, Y.; Nookuea, W.; Li, H.; Thorin, E.; Yan, J. Property impacts on Carbon Capture and Storage (CCS) processes: A review. *Energy Convers. Manag.* **2016**, *118*, 204–222. . [CrossRef]
8. Peres, C.B.; Resende, P.M.R.; Nunes, L.J.R.; Morais, L.C.d. Advances in Carbon Capture and Use (CCU) Technologies: A Comprehensive Review and CO_2 Mitigation Potential Analysis. *Clean Technol.* **2022**, *4*, 1193–1207. [CrossRef]
9. Masson-Delmotte, V.; Zhai, P.; Pörtner, H.O.H.O.; Roberts, D.; Skea, J.; Shukla, P.R.; Pirani, A.; Moufouma-Okia, W.; Pidcock, R.; Connors, S.; et al. "Summary for Policymakers" in Global Warming of 1.5 °C. An IPCC Special Report on the Impacts of Global Warming of 1.5 °C above Pre-Industrial Levels and Related Global Greenhouse Gas Emission Pathways, in the Context of Strengthening the Global Response to the Threat of Climate Change, Sustainable Development, and Efforts to Eradicate Poverty. In *Sustainable Development, and Efforts to Eradicate Poverty*; Technical Report; IPCC: Geneva, Switzerland, 2018.
10. Halkos, G.E.; Gkampoura, E.C. Reviewing Usage, Potentials, and Limitations of Renewable Energy Sources. *Energies* **2020**, *13*, 2906. [CrossRef]
11. Chiari, L.; Zecca, A. Constraints of fossil fuels depletion on global warming projections. *Energy Policy* **2011**, *39*, 5026–5034. [CrossRef]
12. Global Energy Monitor. Global Coal Plant Tracker. Available online: www.globalenergymonitor.org (accessed on 22 March 2023).
13. Bilgili, F.; Koçak, E.; Bulut, Ü.; Kuşkaya, S. Can biomass energy be an efficient policy tool for sustainable development? *Renew. Sustain. Energy Rev.* **2017**, *71*, 830–845. [CrossRef]

14. Sebastián, F.; Royo, J.; Gómez, M. Cofiring versus biomass-fired power plants: GHG (Greenhouse Gases) emissions savings comparison by means of LCA (Life Cycle Assessment) methodology. *Energy* **2011**, *36*, 2029–2037. [CrossRef]
15. Demirbas, A. Combustion characteristics of different biomass fuels. *Prog. Energy Combust. Sci.* **2004**, *30*, 219–230. [CrossRef]
16. Akella, A.; Saini, R.; Sharma, M. Social, economical and environmental impacts of renewable energy systems. *Renew. Energy* **2009**, *34*, 390–396. [CrossRef]
17. Variny, M.; Varga, A.; Rimár, M.; Janošovský, J.; Kizek, J.; Lukáč, L.; Jablonský, G.; Mierka, O. Advances in Biomass Co-Combustion with Fossil Fuels in the European Context: A Review. *Processes* **2021**, *9*, 100. [CrossRef]
18. Xu, Y.; Yang, K.; Zhou, J.; Zhao, G. Coal-Biomass Co-Firing Power Generation Technology: Current Status, Challenges and Policy Implications. *Sustainability* **2020**, *12*, 3692. [CrossRef]
19. Nawaz, Z.; Ali, U. Techno-economic evaluation of different operating scenarios for indigenous and imported coal blends and biomass co-firing on supercritical coal-fired power plant performance. *Energy* **2020**, *212*, 118721. [CrossRef]
20. Tzelepi, V.; Zeneli, M.; Kourkoumpas, D.S.; Karampinis, E.; Gypakis, A.; Nikolopoulos, N.; Grammelis, P. Biomass Availability in Europe as an Alternative Fuel for Full Conversion of Lignite Power Plants: A Critical Review. *Energies* **2020**, *13*, 3390. [CrossRef]
21. Bunn, D.W.; Redondo-Martin, J.; Muñoz-Hernandez, J.I.; Diaz-Cachinero, P. Analysis of coal conversion to biomass as a transitional technology. *Renew. Energy* **2019**, *132*, 752–760. [CrossRef]
22. Keller, V.; Lyseng, B.; English, J.; Niet, T.; Palmer-Wilson, K.; Moazzen, I.; Robertson, B.; Wild, P.; Rowe, A. Coal-to-biomass retrofit in Alberta–value of forest residue bioenergy in the electricity system. *Renew. Energy* **2018**, *125*, 373–383. [CrossRef]
23. De Meulenaere, R.; Maertens, T.; Sikkema, A.; Brusletto, R.; Barth, T.; Blondeau, J. Energetic and Exergetic Performances of a Retrofitted, Large-Scale, Biomass-Fired CHP Coupled to a Steam-Explosion Biomass Upgrading Plant, a Biorefinery Process and a High-Temperature Heat Network. *Energies* **2021**, *14*, 7720. [CrossRef]
24. Rubinstein, R.Y.; Kroese, D.P. *Simulation and the Monte Carlo Method*; John Wiley & Sons: New York, NY, USA, 2016; Volume 10.
25. Sudret, B. Polynomial chaos expansions and stochastic finite-element methods. In *Risk and Reliability in Geotechnical Engineering*; CRC Press: Boca Raton, FL, USA, 2014; Chapter 6; pp. 265–300.
26. Deng, Z.; Hu, X.; Lin, X.; Che, Y.; Xu, L.; Guo, W. Data-driven state of charge estimation for lithium-ion battery packs based on Gaussian process regression. *Energy* **2020**, *205*, 118000. [CrossRef]
27. Richard, B.; Cremona, C.; Adelaide, L. A response surface method based on support vector machines trained with an adaptive experimental design. *Struct. Saf.* **2012**, *39*, 14–21. [CrossRef]
28. Rabitz, H.; Aliş, Ö.F. General foundations of high-dimensional model representations. *J. Math. Chem.* **1999**, *25*, 197–233. [CrossRef]
29. Coppitters, D.; De Paepe, W.; Contino, F. Robust design optimization of a photovoltaic-battery-heat pump system with thermal storage under aleatory and epistemic uncertainty. *Energy* **2021**, *229*, 120692. [CrossRef]
30. De Meulenaere, R.; Coppitters, D.; Maertens, T.; Contino, F.; Blondeau, J. Quantifying the impact of furnace heat transfer parameter uncertainties on the thermodynamic simulations of a biomass retrofit. *Therm. Sci. Eng. Prog.* **2023**, *37*, 101592. [CrossRef]
31. Montgomery, D.C. *Design and Analysis of Experiments*; John Wiley & Sons: New York, NY, USA, 2014.
32. Blatman, G. Adaptive Sparse Polynomial Chaos Expansions for Uncertainty Propagation and Sensitivity Analysis. Ph.D. Thesis, Clermont-Ferrand 2, Clermont-Ferrand, France, 2009.
33. Lüthen, N.; Marelli, S.; Sudret, B. Sparse polynomial chaos expansions: Literature survey and benchmark. *SIAM/ASA J. Uncertain. Quantif.* **2021**, *9*, 593–649. [CrossRef]
34. Donoho, D.L. Compressed sensing. *IEEE Trans. Inf. Theory* **2006**, *52*, 1289–1306. [CrossRef]
35. Blatman, G.; Sudret, B. Adaptive sparse polynomial chaos expansion based on least angle regression. *J. Comput. Phys.* **2011**, *230*, 2345–2367. [CrossRef]
36. Abraham, S.; Raisee, M.; Ghorbaniasl, G.; Contino, F.; Lacor, C. A robust and efficient stepwise regression method for building sparse polynomial chaos expansions. *J. Comput. Phys.* **2017**, *332*, 461–474. [CrossRef]
37. *THERMOFLEX*, version 30; Thermoflow Inc.: Southborough, MA, USA, 2023. Available online: www.thermoflow.com (accessed on 30 April 2023).
38. Abelha, P.; Cieplik, M.K. Evaluation of steam-exploded wood pellets storage and handling safety in a coal-designed power plant. *Energy Fuels* **2021**, *35*, 2357–2367. [CrossRef]
39. Fosnacht, D.R.; Hendrickson, D.W. *Use of Biomass Fuels in Global Power Generation with a Focus on Biomass Pre-Treatment*; Technical Report; Natural resources research institute, University of Minnesota Duluth: Duluth, MN, USA, 2016.
40. Lam, P.S. Steam Explosion of Biomass to Produce Durable Wood Pellets. Ph.D. Thesis, The University of British Columbia, Vancouver, BC, Canada, 2011.
41. Løhre, C.; Underhaug, J.; Brusletto, R.; Barth, T. A Workup Protocol Combined with Direct Application of Quantitative Nuclear Magnetic Resonance Spectroscopy of Aqueous Samples from Large-Scale Steam Explosion of Biomass. *ACS Omega* **2021**, *6*, 6714–6721. [CrossRef] [PubMed]
42. Blondeau, J.; Van den Auweele, J.; Alimuddin, S.; Binder, F.; Turoni, F. Online adjustment of Furnace Exit Gas Temperature field using advanced infrared pyrometry: Case study of a 1500 MWth utility boiler. *Case Stud. Therm. Eng.* **2020**, *21*, 100649. [CrossRef]
43. Ozer, M.; Basha, O.M.; Stiegel, G.; Morsi, B. 7—Effect of coal nature on the gasification process. In *Integrated Gasification Combined Cycle (IGCC) Technologies*; Wang, T., Stiegel, G., Eds.; Woodhead Publishing: Sawston, UK, 2017; pp. 257–304.

44. Miller, B.G. 4—Introduction to Coal Utilization Technologies. In *Clean Coal Engineering Technology*, 2nd ed.; Miller, B.G., Ed.; Butterworth-Heinemann: Oxford, UK, 2017; pp. 147–229.
45. Coppitters, D.; Tsirikoglou, P.; De Paepe, W.; Kyprianidis, K.; Kalfas, A.; Contino, F. RHEIA: Robust design optimization of renewable Hydrogen and dErIved energy cArrier systems. *J. Open Source Softw.* **2022**, *7*, 4370. [CrossRef]
46. Coppitters, D.; De Paepe, W.; Contino, F. Robust design optimization and stochastic performance analysis of a grid-connected photovoltaic system with battery storage and hydrogen storage. *Energy* **2020**, *213*, 118798. [CrossRef]
47. Verleysen, K.; Parente, A.; Contino, F. How does a resilient, flexible ammonia process look? Robust design optimization of a Haber-Bosch process with optimal dynamic control powered by wind. *Proc. Combust. Inst.* **2023**, *39*, 5511–5520. [CrossRef]
48. Liang, H.; Hua, H.; Qin, Y.; Ye, M.; Zhang, S.; Cao, J. Stochastic Optimal Energy Storage Management for Energy Routers via Compressive Sensing. *IEEE Trans. Ind. Inform.* **2022**, *18*, 2192–2202. [CrossRef]